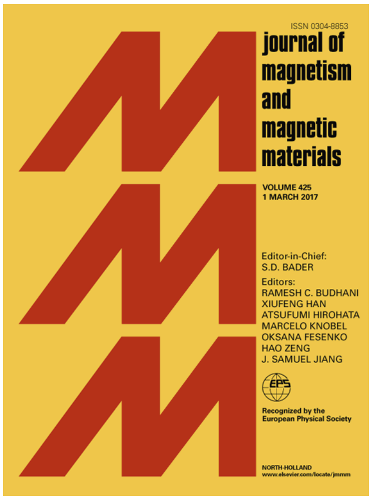

Controlling the crystalline and magnetic texture in sputtered $Fe_{0.89}$ $Ga_{0.11}$ thin films: influence of substrate and thermal treatment

G.A. Ramírez, F. Malamud, J.E. Gómez, L.M. Rodríiguez, D. Fregenal, A. Butera, J. Milano

PII: S0304-8853(18)34132-5
DOI: https://doi.org/10.1016/j.jmmm.2019.03.099
Reference: MAGMA 65114

To appear in: *Journal of Magnetism and Magnetic Materials*

Please cite this article as: G.A. Ramírez, F. Malamud, J.E. Gómez, L.M. Rodríiguez, D. Fregenal, A. Butera, J. Milano, Controlling the crystalline and magnetic texture in sputtered $Fe_{0.89}$ $Ga_{0.11}$ thin films: influence of substrate and thermal treatment, *Journal of Magnetism and Magnetic Materials* (2019), doi: https://doi.org/10.1016/j.jmmm.2019.03.099

Controlling the crystalline and magnetic texture in sputtered $Fe_{0.89}Ga_{0.11}$ thin films: influence of substrate and thermal treatment

G. A. Ramírez,[1,2] F. Malamud,[2,3] J. E. Gómez,[1]
L. M. Rodríguez,[3] D. Fregenal,[3] A. Butera,[1,2] and J. Milano[1,2]
[1]*Instituto de Nanociencia y Nanotecnología,*
CNEA-CONICET. Centro Atómico Bariloche,
(R8402AGP) San Carlos de Bariloche, Argentina
[2]*Universidad Nacional de Cuyo, Instituto Balseiro. Centro Atómico Bariloche,*
(R8402AGP) San Carlos de Bariloche, Argentina.
[3]*CNEA-CONICET, Centro Atómico Bariloche,*
(R8402AGP) San Carlos de Bariloche, Argentina

(Dated: February 6, 2019)

Abstract

In this work we present a careful study on the relationship between the magnetic and structural properties of a highly magnetostrictive $Fe_{0.89}Ga_{0.11}$ (Fe-Ga) alloy deposited onto glass, Si and MgO substrates. When grown on glass, the films are polycrystalline with randomly oriented grains without any texture, while the ones on Si and MgO present preferred growth directions. Fe-Ga/Si films show a [113] fibre-like texture, and Fe-Ga/MgO presents a quasi monocrystalline behavior with the (100) film plane direction parallel to the substrate surface. When Fe-Ga/MgO films are annealed an additional (110) texture is also observed. Magnetometry and ferromagnetic resonance (FMR) show that the magnetic behavior is closely related to the structural observed textures. Furthermore, the structural analysis allowed us to get a deeper understanding of the magnetic behavior. This point is very important to get the ability of controlling the crystalline texture by means of growing onto different substrates and/or thermal treatments, which in turns opens the possibility of handling the magnetic texture which is particularly important in magnetostrictive materials for electronic devices.

I. INTRODUCTION

Size reduction is one of the premises of the electronic industries besides the attainment of faster devices, the reduction of energy comsuption and the increase in storage capacity. Specifically, in micro and nano magnetic devices for data storage, the control of magnetization gives a new degree of freedom for reaching the above mentioned properties[1]. One of the possibilities for the magnetization handling is to use the magnetoelastic coupling (MEC), which one of its macroscopic and well known properties is the magnetostriction[2]. This gives account for the size change of a ferromagnetic material when a magnetic field is applied. Also, the reciprocal effect is observed, i.e., by appling a mechanical stress to a magnetostrictive material its magnetic state can be changed. In the literature, this method to control the state of a device is usually named as straintronics[3–5]. In this manner, it is possible to handle the magnetic properties by a controlled mechanical deformation. A promising material in which the magnetization piloting is interesting to explore is the $\mathrm{Fe}_{1-x}\mathrm{Ga}_x$ alloy. This ferromagnetic metal, usually called Galfenol, presents a huge magnetostriction, with a maximum $\frac{3}{2}\lambda_{100} \sim 395\times10^{-6}$ (more than one order of magnitude higher than Fe), which is observed for $x \sim 0.19$ as reported in Ref. 6.

Several technological applications require that materials be grown as thin films. The crystalline grain structure of such films can vary from a polycrystaline structure to a monocrystalline one depending on the fabrication technique, deposition conditions, post-growth thermal treatments and the type of substrate. The crystallographic orientation of the grains in polycrystalline films is also often non-random, even when they are deposited on amorphous substrates, i.e., the grains tend to align along specific crystallographic planes parallel to the substrate (crystallographic texture)[7]. The grain geometry, the average grain size, the grain size distribution and the distribution of grain orientations in polycrystalline films strongly affect their properties, in particular the magnetic ones.

The precise control of the structural texture by a deep knowledge of the deposition conditions, post-growth thermal treatments and substrate structure could be used to tailor samples with desired magnetic properties. Specifically, in $\mathrm{Fe}_{1-x}\mathrm{Ga}_x$ magnetostrictive thin films, tailoring could lead to combine the magnetoelastic coefficients present in the material[2] and, in this way, to handle the magnetostrictive response of the film.

$\mathrm{Fe}_{1-x}\mathrm{Ga}_x$ thin films could be grown through several techniques, e.g., electrodeposition[8], molecular beam epitaxy[9] and sputtering[10]. Many works have been devoted to understand either the structural properties or the magnetic ones[11–13]. However, a careful study on how both aspects (magnetic and structural) are linked is still lacking, even more if we take into account that this material presents a high MEC. Besides getting a deeper understanding of the physical properties, a succesful determination of such a relationship could be important to develop materials where the magnetostriction can be tuned according to the needs via controlling their microstructure.

In this work we present a detailed study of the structural and magnetic properties of $\mathrm{Fe}_{1-x}\mathrm{Ga}_x$ ($x = 0.11$) thin films as-grown and thermally annealed. Such films were grown onto different substrates: glass, Si(100) and MgO(100), with the aim to correlate the crystalline texture with the magnetic properties.

II. EXPERIMENTAL

$\mathrm{Fe}_{0.89}\mathrm{Ga}_{0.11}$ thin films with a nominal thickness of 200 nm were fabricated by dc magnetron sputtering on glass and on single-crystals of naturally oxidized Si(100) and MgO(100). The samples were deposited from a 3.8-cm diameter Fe-Ga alloy target with a Ga nominal atomic composition, $x = 0.17$. The film growth was carried out at room temperature with the following deposition conditions: base pressure $<1.5\times10^{-6}$ Torr, sputtering power 20 W, argon pressure 3 mTorr, and deposition rate 0.136 nm/s. The annealing procedure consisted in increasing the sample temperature to 250°C, holding during 2 hours in the growing chamber and, then, cooling down to room temperature in 2 hours. The Fe and Ga concentration in the target and the films was determined by means of X-ray photoelectron spectroscopy (XPS), Rutherford backscattering (RBS), energy dispersive X-ray spectrometry (EDX) and particle induced X-ray emission (PIXE). The RBS and PIXE measurementes were carried out in a NEC 1.7 MeV Tandem accelerator with a NEC RC43 high vaccum end station attached, using 2 MeV He^+ ions for RBS and 3 MeV H^+ for PIXE[14]. Analysis of RBS spectra were done using SIMNRA software[15], while GUPIX software[16] was used to analyse PIXE spectra. The crystalline structure was determined either by using a Bruker D8 Advance diffractometer with rotating sample holder or a Panalytical Empyrean diffractometer with an eulerian craddle, both with a Cu X-ray tube ($\lambda_{K_\alpha}\mathrm{Cu} = 0.15418$ nm). The first diffractometer allowed us to determine accurately the lattic parameters of the target and Fe-Ga films grown onto glass. The second one was used to determine the lattice parameters for Fe-Ga grown on Si and MgO, as well as the pole figures for texture analysis by using the eulerian cradle. The magnetometry study was performed by a superconducting quantum interference device (SQUID) and a vibration sample magnetometer (VSM) with an applied field H along several in-plane angles ϕ_H. Magnetic anisotropies were determined by ferromagnetic resonance (FMR) at a excitation frequency $\nu \sim 24$ GHz (K-band). For this purpose, we performed angular measurements in the film plane with the aim of obtaining the relationship between the resonance field, H_r, at different in-plane film directions. All the magnetic measurements were done at room temperature.

III. RESULTS AND DISCUSSION

A. Composition

All the used techniques for determining the composition give coincidental results. In Fig. 1(a), it is possible to see a typical spectrum of a Fe-Ga film grown on Si substrate and its analysis through the SIMNRA software. The information provided by RBS for all the samples indicates that their composition is the same in any case, with an atomic ratio of (0.11 ± 0.02) Ga and (0.89 ± 0.02) Fe. These values were confirmed by XPS, PIXE and EDS. In addition, the RBS shows that the concentration ratio is constant through the entire layer with no gradient. Also, there is a minor but expectable overlaping in the interfacial zone due to the roughness of the substrate, this overlaping is evidenced in the "tail" located at the baseline of the spectrum, to the left of the film steps and to the right of the Si plateau. We also measured the chemical composition of the target with PIXE, which is suitable for characterizing metal samples[17]. We have found a Ga concentration of $x_{\text{tgt}} = (0.14 \pm 0.02)$, being greater than the concentration obtained for the films ($x_{\text{film}} = 0.11$) but lower than the nominal concentration informed by the target supplier.. The Fig. 1(b) shows the PIXE spectrum of the target and its analysis using GUPIX software. In order to search for possible concentration anisotropies that may lead to the shortage of Ga observed in the films, we mapped the target surface. However it shows an uniform composition within the uncertainty of PIXE (<2%).

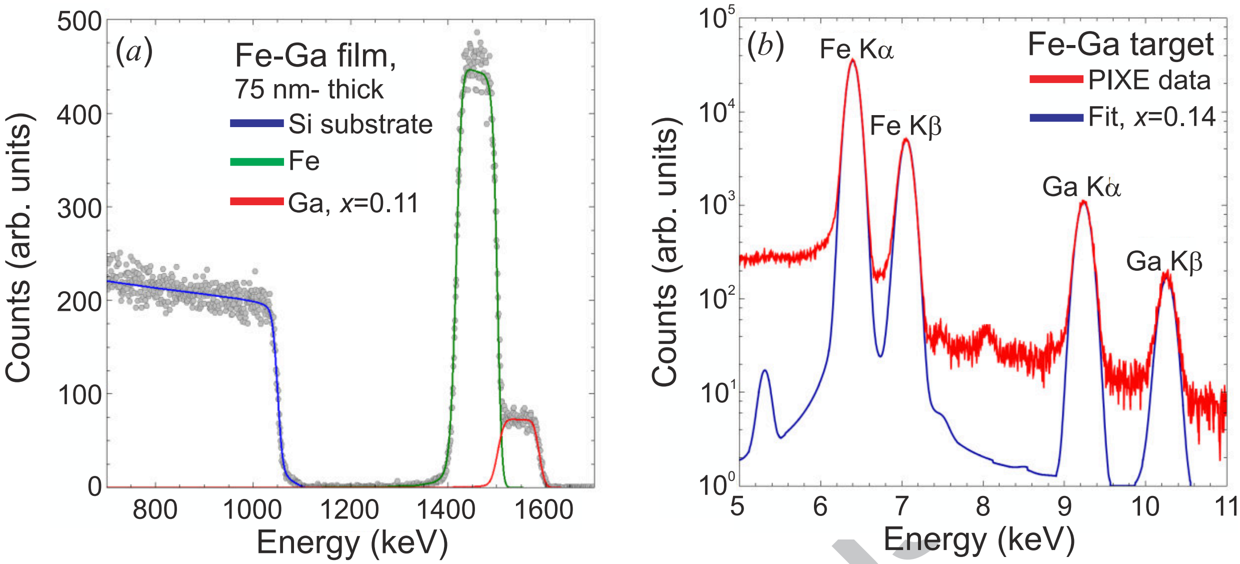

FIG. 1. (a) RBS spectrum for a 75-nm thick Fe-Ga film and the best fitting curve by using the SIMNRA code. (b) PIXE spectrum for the Fe-Ga target and the best fittng curve trough the GUPIX software

B. Structural

The lattice parameter of the sputtering target, a_{tgt}, was determined in a bcc-like cubic structure being $a_{\mathrm{tgt}} = (0.2912 \pm 0.0004)$ nm, which is larger than the lattice parameter reported in Ref. 18 for the same concentration ($a_{\mathrm{Bulk}} = 0.290$ nm for $x = 0.17$). Also, the lattice parameter of Fe-Ga grown on glass, a_{gl} was determined to be $a_{\mathrm{gl}} = (0.2886 \pm 0.0005)$ nm. As already mentioned in Sec. III A, this difference can be explained by a reduction of the Ga concentration if stress imposed by the substrate are not taken into account.

The structure of Fe-Ga films was also studied by X-ray diffractometry performing conventional Bragg-Brentano θ-2θ scans (2θ is the angle between the incident and the diffracted beams) using an eulerian cradle for the determination of the interplanar distances d_{hkl}. The advantage of using an Eulerian craddle was to shift the angle of the diffraction with respect to the film normal to avoid the superposition of the film and the substrate peaks. Fig. 2(a) shows the indexed diffractograms for the different studied samples, measured for a direction rotated 30° from the sample normal (growth direction),i.e., (110), (200), (211) and (220) diffraction reflections can be resolved. The diffractograms were refined by a simple full pattern Rietveld-type refinement model that has been developed to extract accurate lattice parameters from a single XRD measurement of a textured multiphase sample. The method has been recently applied to study the composition dependence of lattice parameters of the austenite (FCC) and the martensitic structures (BCC and HCP) of Fe-Mn-Cr alloys[19]. As an example of the fitting procedure, Fig. 2 shows the indexed X-ray pattern obtained for the Fe-Ga/glass as grown sample in the normal direction with the corresponding data refinement. The lower blue line plot shows the differences between measured and fitted intensities. As can be appreciated from the residual curve, the fitting is very good.

TABLE I. Lattice parameters of the films and the target.

Substrate	Lattice parameter (nm)	
	As-grown	Annealed
Sputtering target	0.2912 ± 0.0004	
Glass	0.2886 ± 0.0005	0.2871 ± 0.0005
Si	0.289 ± 0.002	0.289 ± 0.001
MgO	0.289 ± 0.002	0.288 ± 0.001

C. Pole figures

The crystallographic texture of the samples was obtained for the (110), (200) and (211) reflections[20]. From the experimental pole figures, the recalculated pole figures (RPF) and the orientation distribution function (ODF) was determined using the MTEX code[21]. We briefly introduce how ODF is calculated by using MTEX in Appendix. Fig. 3 shows the RPF for the as-grown and annealed Fe-Ga/glass and Fe-Ga/Si samples respectively, in the same color scale. As we can observe in Fig. 3(a) and (b), both figures present similar characteristics, indicating that the annealing treatment does not produce appreciable changes in the microstructure. The differences among maxima and minima of the RPF intensities are within the accuracy of the method. This indicates that Fe-Ga/glass does not present any preferential texture, therefore the crystallites are randomly distributed.

The RPF results for Fe-Ga/Si are displayed in Fig. 3(*c*) and (*d*) for the as-grown and annealed samples, respectively. The RPF for Fe-Ga/Si shows a typical fibre-like texture, where

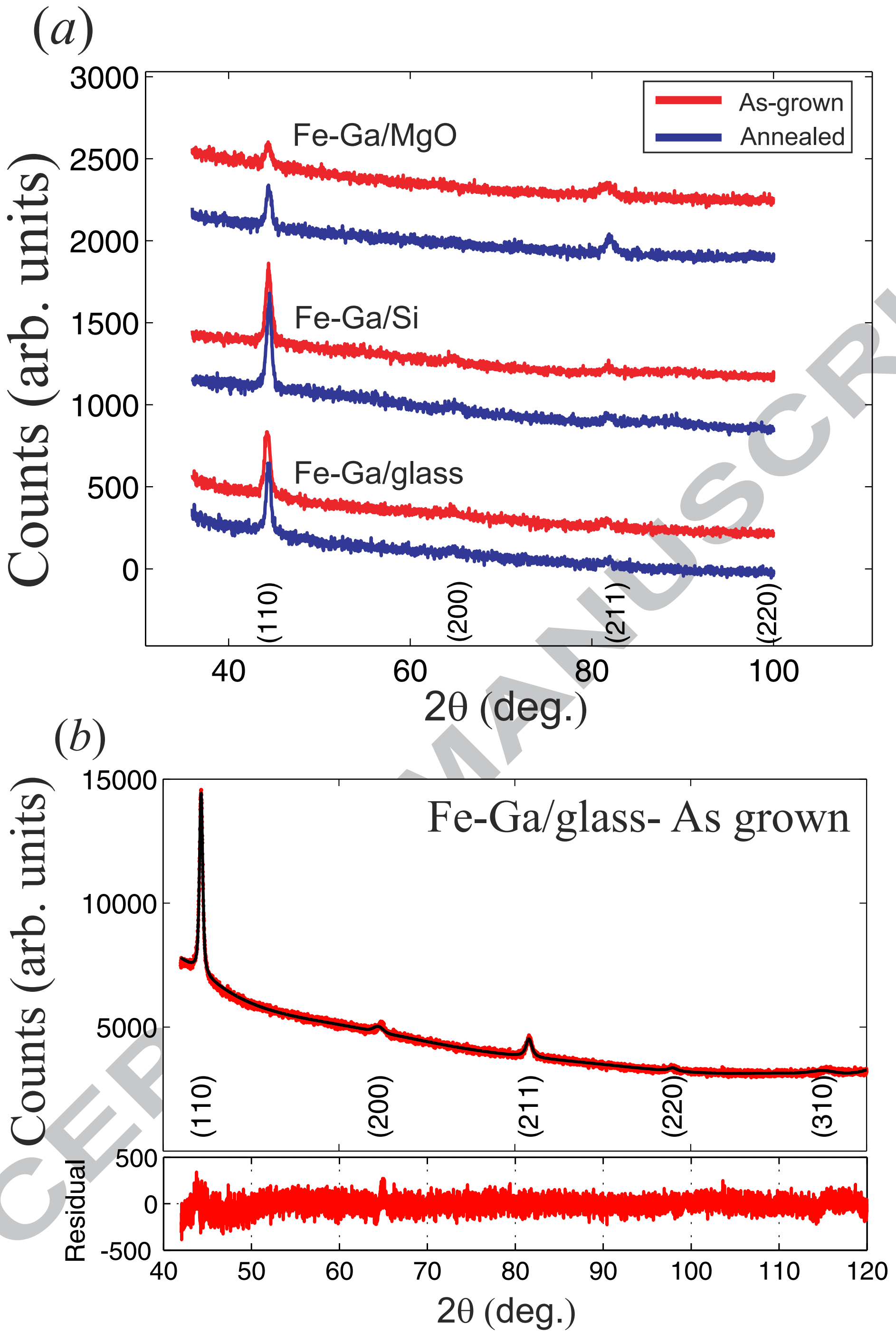

FIG. 2. (*a*) Diffractograms for the studied samples measured at 30° from the sample normal. (*b*) Indexed X-ray pattern obtained for the Fe-Ga/glass - as grown sample in the normal direction (red dots), the solid black lines corresponds to the data fit of such refinements and the lower red line plot shows the differences between measured and fitted intensities.

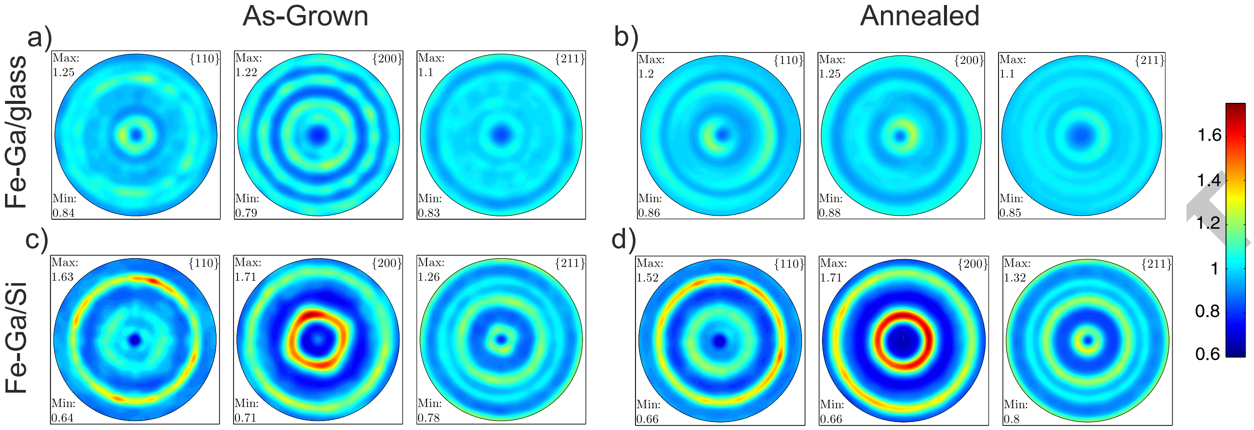

FIG. 3. (*a*) and (*b*) RPF for as-grown and annealed Fe-Ga/glass samples, respectively. (*c*) and (d) RPF for as-grown and annealed Fe-Ga/Si samples, respectively.

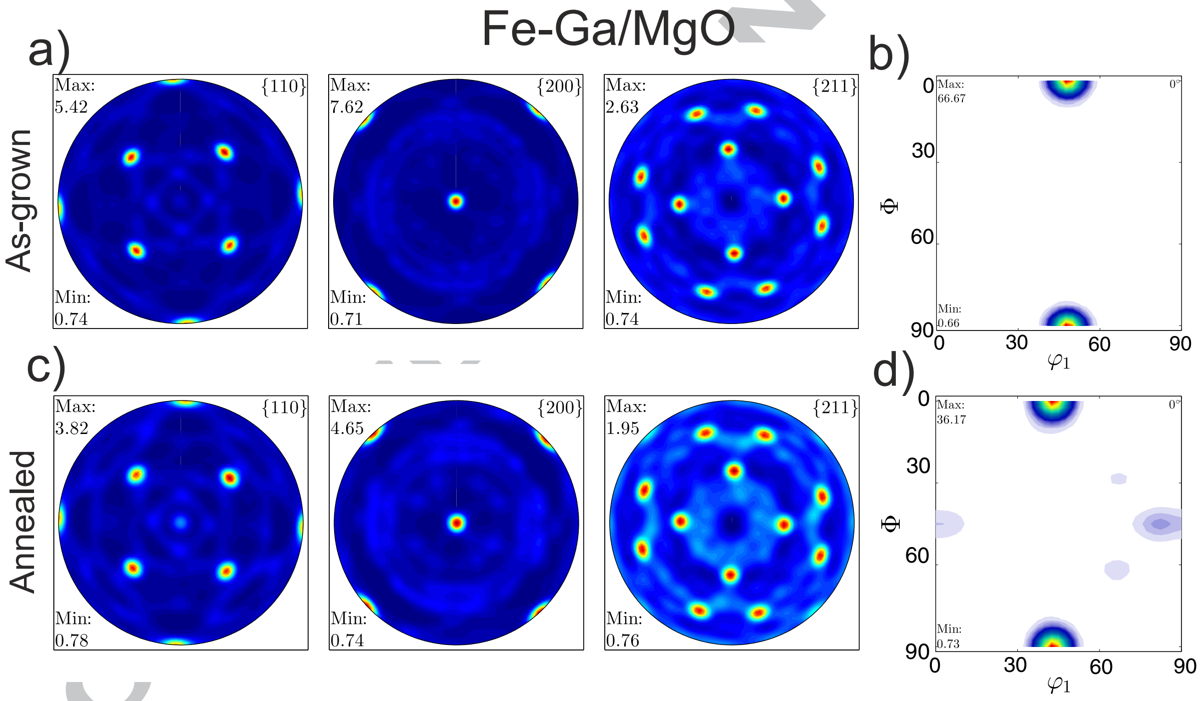

FIG. 4. (a) and (c) RPF for the indicated directions for Fe-Ga/MgO as-grown and annealed samples, respectively. (b) and (d) ODF plot at $\phi_2 = 0°$ for the Fe-Ga/MgO as-grown and annealed samples, respectively.

the {113} are oriented normally to the film plane and the {200} are randomly distributed at 30° with respect to the film normal for the as-grown and annealed samples. Both samples present the same principal texture component, labelled {113}<001> fibre, with volume fractions of 8.6% and 10.3% for the as-grown and annealed samples, respectively. The volume fractions were computed using MTEX for the crystals with a maximum missorientation of 8° from the {113}<001> fibre. In this way, the only observed effect due to the annealing was to increase slightly the texture volume fraction, showing that the thermal treatment favours the realignment of the crystallite to the mentioned component texture. The rest of the volume does not present a preferred texture (randomly oriented crystallites).

In order to predict theoretically the textures arising in metallic thin films, the simple models identify two contributions that compete energetically[22]. One of these two contributions is the elastic energy, which makes films grow along the crystalline direction that minimizes the elastic film energy when the sample is under stress. Tipically, this stress arises usually from misfit, thermal expansion or modified surface strain in the substrate[23–25]. Considering a bcc structure of a film grown onto an amorphous substrate, the elastic energy term predicts a dominant texture (100) or (111) along the growth direction, depending on the composition of the film[23]. On the other hand, the surface energy term favours a growth that follows the closest packed direction, being the (111) and (110) for fcc and bcc lattices, respectively[22]. When these two terms compete it is expected that for thinner films (<100 nm) the surface energy is dominant, while for thicker ones (>100 nm) the elastic term prevails[23]. However, in most cases, these models do not predict the measured textures[22,24] as it happens in our samples. This issue suggests that the attained equilibrium texture depends on other variables as well. Generally, they are related to the type of substrate, growth conditions, post-growth treatments which, finally, modify the energetic balance.

Present models made for films grown on amorphous substrates show how the texture is dinamically modified during growth and that the resulting microstructure depends mainly on the film thickness and substrate temperature[7,26]. Particularly, the derived temperature structure zone model, DTSZM[27,28] takes only into account the substrate temperature to study the microstructure evolution. The relevant parameter is the T_s/T_m ratio, which relates the substrate temperature during growth, T_s, and the bulk melting point of the material, T_m. Basically, DTSZM consists of three temperture zones, i.e., $T_s/T_m < 0.1$, $0.1 < T_s/T_m < 0.3$ and $T_s/T_m > 0.3$. Taking into account that the samples were grown at room temperature ($T_s \sim 300$ K) and the bulk melting point is $T_m \sim 1500$ K, they are at the second zone, $0.1 < T_s/T_m < 0.3$, usually called competitive texture zone or T zone. This T zone is characterized by the fact that the microstructure depends on the film thickness. For thinner films a small grain structure exists with a random orientation of crystals without any preference of a given domain orientation, as it is observed for the Fe-Ga/glass samples. This fact indicates that the main phenomenon which governs the microstructure evolution in the post-nucleation range is crystal growth, i.e., the system presents a high density of nucleation centers and, at these nuclei, the first growing crystals are randomly oriented on the amorphous substrate. Moreover, at this stage there is no grain boundary mobility; consequently the continuous film developing at first on the substrate is composed of randomly oriented crystals[27].

Fe-Ga/Si samples show that a small volume fraction of the thin film has a texture component with the relationship i.e. {113}<001>. This would indicate that, in spite of being in the same T region as Fe-Ga/glass samples, Fe-Ga/Si films are characterized by the orientation controlled growth competition of the randomly oriented crystals, resulting in orientation selection. Crystals with faster growing faces (low adatom mobility) accumulate more adatoms by surface diffusion from the neighbour crystals oriented with high adatom mobility faces and will grow over them. Altough the texture volume in Fe-Ga/Si(100) is small ($\sim$ 10%), it is important to note that differences in texture are not expected in the films on glass and on Si(100) because they were grown at the same deposition conditions. Probably, the differences in thermal conductivities and surface roughness of the substrates may lead to this behavior. Note also that the observed texture of Fe-Ga/Si does not agree with the preferred direction due to surface energy minimization for bcc structures, i.e., (110); however, the observed {113} texture is close to (001), which was already reported in Cr onto NiP-coated AlMg substrates[29,30].

Fig. 4 displays the RPF and ODF sections for the as-grown and annealed Fe-Ga/MgO samples. As it is shown in Fig. 4(a), the as-grown sample presents a monocrystalline texture component which can be characterized by the Euler angles $(\varphi_1,\Phi,\varphi_2) = (45°,0°,0°)$ [Fig. 4(b)] using the Bunge convention[31]. The crystal orientation with respect to the substrate is $(001)_{\mathrm{Fe-Ga}} \parallel (001)_{\mathrm{MgO}}$ and $[100]_{\mathrm{Fe-Ga}} \parallel [110]_{\mathrm{MgO}}$, matching with orientations already reported[32,33]. Considering that $a_{\mathrm{MgO}} = 0.4203$ nm and $\sqrt{2}\,a_{\mathrm{Fe-Ga}} = 0.409$ nm, we have that the film suffers an tensile stress of 2.8%. The corresponding volume fraction of this crystalline orientation is 80%, computed by MTEX using a 8° radius sphere centered at the (45°,0°,0°) orientation. The rest of the sample (20%) presents a non textured structure (randomly oriented crystallites). Fig. 4(c) shows the RPF for the Fe-Ga/MgO annealed sample. In this figure, we observe that the principal texture orientation is preserved with respect to the as-grown sample, with a volume fraction of 67%. However, the ODF section displayed in Fig. 4(d) reveals a new weaker texture component with Euler angles which are aligned $(110)_{\mathrm{Fe-Ga}} \parallel (001)_{\mathrm{MgO}}$ and $[001]_{\mathrm{Fe-Ga}} \parallel [100]_{\mathrm{MgO}}$. This new component presents a volume fraction of 27% also computed by MTEX using a 8° radius sphere centered at the (0°,55°,0°) orientation. The remaining volume fraction, 6%, is not textured (randomly oriented crystallites).

An analysis of the elastic strain energy due to the lattice misfit between the film and substrate[25] at the interface predicts the epitaxy we have observed, i.e., $(001)_{\mathrm{Fe-Ga}} \parallel (001)_{\mathrm{MgO}}$ and $[100]_{\mathrm{Fe-Ga}} \parallel [110]_{\mathrm{MgO}}$. On the other hand, the crystallographic directions defined by the (110) epitaxy do not match with those arising from the criterion of minimizing the misfit elastic energy. This would indicate that the origin of this texture is not the epitaxy at the interface. However, it is interesting to note that the observed (110) texture is the expected one when surface energy dominates in bcc systems because the (110) plane is the more compact one[22]. The fact that the volume of this texture grows after annealing may indicate that the surface term is energetically more favorable than the strain arising from the epitaxy at the interface[34].

D. Magnetic structure

1. *Fe-Ga/glass samples*

In Fig. 5(a) and (b), we show hysteresis loops for the as-grown and annealed Fe-Ga/glass films respectively, where H was applied at several in-plane substrate directions, ϕ_H. The measured saturation magnetization for these samples and the rest of the films is $M_s = (1500 \pm 100)\times 10^3$ A/m, in agreement with M_s for bulk Fe-Ga of the same concentration[35]. In the figure corresponding to the as-grown sample [Fig. 5(a)], we can observe that the coercive field, $\mu_0 H_c$ [where μ_0 is the vacuum permeability, $\mu_0 = 4\pi\times 10^{-7}$ Tm/A)], varies from 1.3 to 2.1 mT and the normalized remnant magnetization M_r/M_s from 0.67 to 0.89, where the maxima of $\mu_0 H_c$ and M_r/M_s are found for $\phi_H = 0°$. This indicates the presence of a small uniaxial anisotropy, probably related to spatial inhomogeneites during the sputtering process. This point will be studied in more detail later in the FMR analysis. Fig. 5(*b*) displays the hysteresis loops for the annealed Fe-Ga/glass sample. The observed behaviour for this sample is similar to the as-grown one, showing also an uniaxial anisotropy. However, the coercive field presents smaller values with respect to the as-grown sample, suggesting a decrease in the number and/or nature of pinning centers that play a role in the domain wall movement.

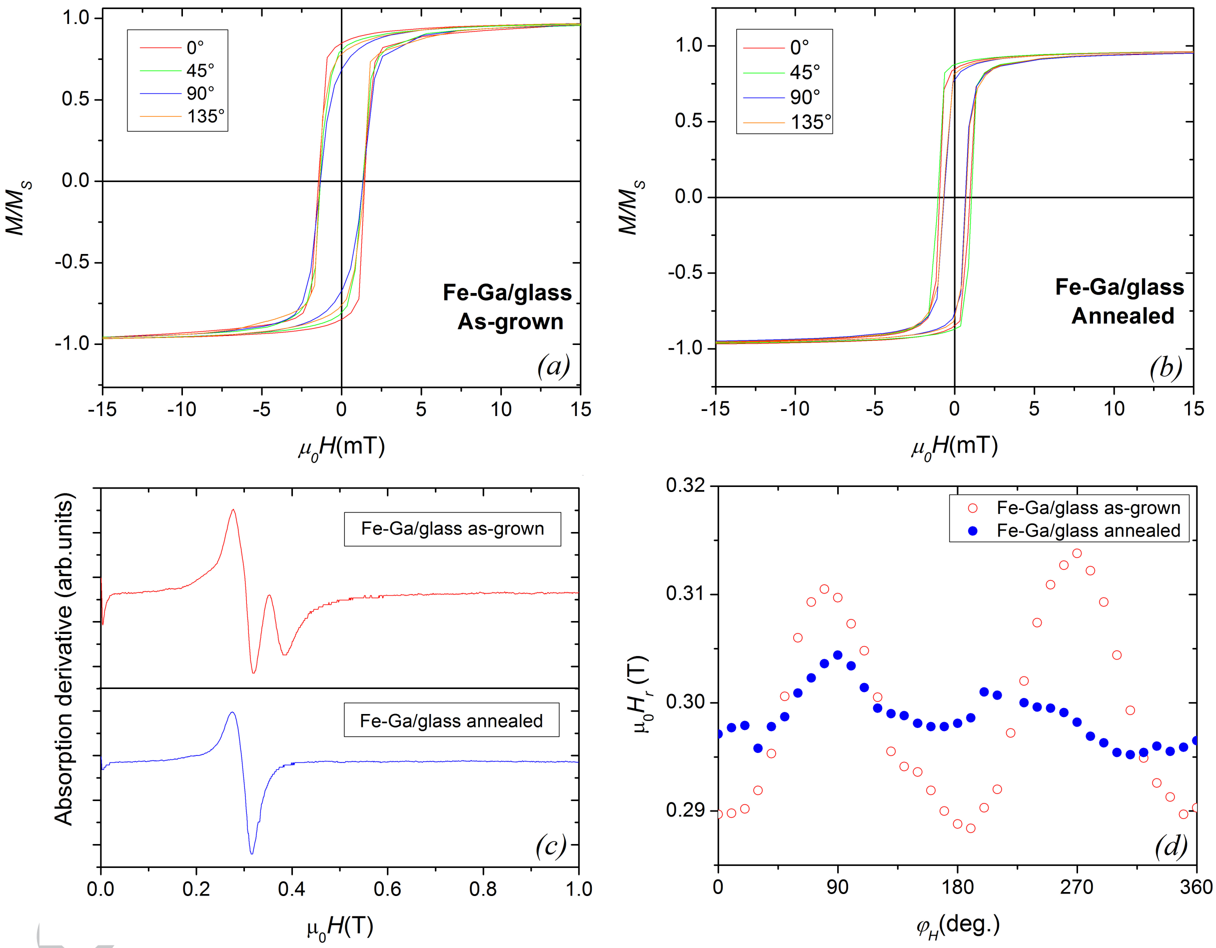

FIG. 5. In-plane M *vs.* H loops for the as-grown (*a*) and annealed (*b*) Fe-Ga/glass films. (*c*) FMR spectra for the as-grown (top panel) and annealed (bottom panel) samples at $\phi_H = 60°$. (*d*) H_r as a function of ϕ_H for the as-grown and annealed samples.

Fig. 5(c) displays the FMR spectra at a given fixed azimuthal angle, ϕ_H, for the as-grown and annealed Fe-Ga/glass samples. The spectrum belonging to the as-grown sample (top panel) shows two modes: a larger one at low fields and a satellite peak shifted to higher fields. The appearence of more than one mode indicates the presence of regions with different magnetic response. Such regions have different effective magnetic anisotropies and this is reflected in the observed split of the resonance fields. After annealing (bottom panel), Fe-Ga/glass presents just one mode, indicating that the thermal treatment helps to homogenize the magnetic response in the whole sample. Moreover, the annealing leads to a more isotropic magnetic behavior in the film plane. This effect is observed when H_r is plotted as a function of ϕ_H. The smaller variation of H_r along ϕ_H in the annealed case ($\Delta\mu_0 H_r \sim 0.01$ T) with respect to the as-grown one ($\Delta\mu_0 H_r \sim 0.03$ T) indicates that the induced magnetic anisotropy during the growth process could be partially removed.

When samples are grown by sputtering, the existence of an in-plane uniaxial anisotropy depends on the target-substrate alignment as well as the kind of deposition regime. Oblique incidence means that the target and substrate are not aligned. In this condition the spatial symmetry is broken and a uniaxial axis can be observed[36]. However, the strenght of such an anisotropy can be controlled by changing the deposition regime. On the one hand, the ballistic deposition means the atoms ejected from the target reach the substrate preserving their momentum and energy (low collision rate). On the other hand, in the diffusive flow the collision number of the ejected atoms is large enough to thermalize. If the target-substrate distance, d is smaller than the mean free path of ejected atoms, λ, the flow will be ballistic and, on the contrary, if d is larger than λ the regime will be diffusive. In Ref.[36], it is observed that the ballistic flow induces a more ordered structure in the sample than the diffusive regime, hence it is expected that the induced uniaxial anisotropy by the oblique incidence is observed. Conversely, if the sample is grown in the diffusive regime a more disorder structure is observed, which is reflected in the appearence of inhomogeneites within the sample. Such inhomogeneites leads to the appearence of local fluctuations of the anisotropy, which reduces the uniaxial anisotropy. Our samples were grown in the ballistic regime ($\lambda \sim 10$ cm, according to Eq. (1) of Ref. 36 and $d \sim 5$ cm) and the incidence was normal instead of oblique, avoiding, in principle, the appearence of an anisotropy due to the growth process. However, a uniaxial anisotropy was detected. Therefore, we argue that the observed anisotropy arises from either a small misalignment between target and substrate or a plasma inhomogeneity that, taking into account the ballistic regime, finally induces a uniaxial anisotropy in the samples.

2. Fe-Ga/Si sample

In Figs. 6(a) and (b), we show the hysteresis loops for the as-grown and annealed Fe-Ga/Si samples, respectively. Both figures show the presence of a uniaxial anisotropy, where the easy axis is along to the $[1\bar{1}0]_{\mathrm{Si}}$ direction, indicated by the fact that M_r/M_s and H_c values are higher for this direction. The hard axis is along the $[110]_{Si}$ direction, and it is characterized by a lower remnant magnetization and a smaller coercive field. Then, the medium axes are along $[100]_{\mathrm{Si}}$ and $[010]_{\mathrm{Si}}$ as shown in Figs. 6(a) and (b). It is important to note that after the thermal treatment the orientation of the magnetic anisotropy is preserved. However, the annealed sample [Fig. 6(b)] shows a more isotropic behavior compared to the as-grown one [Fig. 6(a)], which is reflected by the fact that M_r and H_c present a smoother variation among the different in-plane directions. Another remarkable fact is that the easy axis is aligned along $[1\bar{1}0]_{\mathrm{Si}}$. Due to the native amorphous oxide present in our Si subtrates, we do not expect an anisotropy induced by the Si substrate. However, our measurements suggest that the magnetic anisotropy direction is related to the substrate orientation.

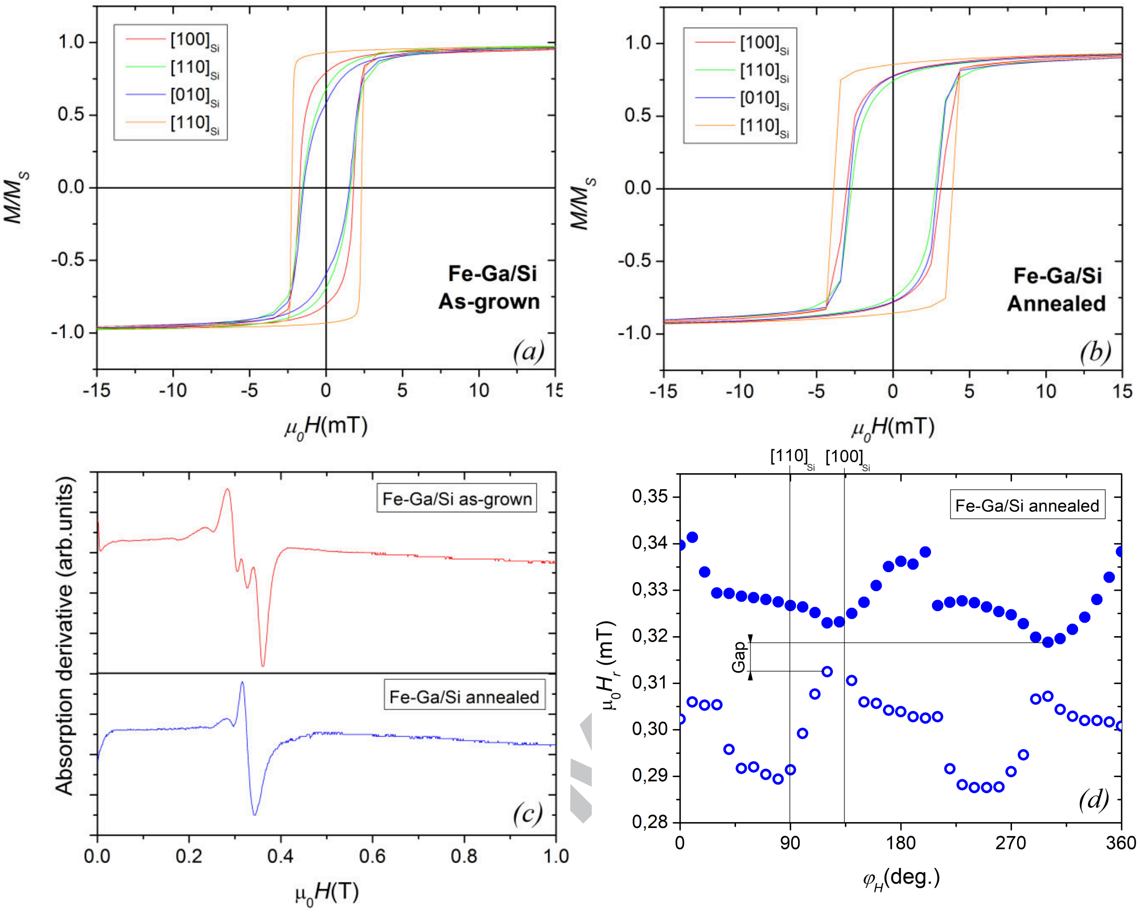

FIG. 6. (a) and (b) In-plane M $vs.$ H loops for the as-grown and annealed Fe-Ga/Si(100) samples. (c) FMR spectra for the as-grown (top panel) and annealed (bottom panel) samples $\phi_H = 60°$. (d) H_r as a function of ϕ_H for the annealed sample.

In Fig. 6(c), we show the FMR spectra at a given fixed azimuthal angle, $\phi_H = 60°$, for the Fe-Ga/Si samples. In this case, the behavior is similar to the Fe-Ga/glass one, i.e., the as-grown sample (top panel) shows a complex structure with at least four peaks and after annealing (bottom panel) only a single peak with a small satellite is observed. This indicates a more homogeneous magnetic behavior. Furthermore, in the as-grown Fe-Ga/Si films, the modes can be related to weak structural anisotropies in the RPF. In Fig. 3(c), left panel, it is possible to observe that the intensity of the circle that corresponds to the fibre-like behavior is not homogeneus: we can detect four zones where the intensity reaches a maximum. This means that this spatial texture anisotropy is reflected as multiple modes in the FMR spectrum. In Fig. 6(d), we show the resonance fields as a function of ϕ_H, corresponding to the two modes observed for the annealed Fe-Ga/Si sample. The absorption lines in Fig. 6(c) do not cross between them, then the upper (lower) mode [red (black) dots] corresponds always to the more (less) intense peak. Both modes are separated by a gap of $\sim$0.01 T from the top of the lower mode to the bottom of the upper one. They also show a two-fold behavior in agreemenet with the hysteresis loops. Moreover, the two modes present fingerprints of interaction between them. On the one hand, the existing gap indicates mode "repulsion" typically observed in coupled systems[37–39]. On the other hand, we also observed an exchange of the mode character: as observed in Fig. 6(d), the lowest H_r values (easy axis) corresponding to the lower mode and the highest H_r values (hard axis) of the upper mode are shifted by 90°. In a monodomain system, this behavior is expected when a uniaxial in-plane anisotropy is present. The fact that, in our case, this behavior is reflected in both modes would indicate the coupling between the two magnetic domains present in the sample.

3. Fe-Ga/MgO(100) samples

In Fig. 7(a), we display the M $vs.$ H loops at different in-plane angles for the as-grown Fe-Ga/MgO(100) sample. This film presents a magnetic anisotropy in the film plane, which is readily seen in the M_r behavior. When H is applied along the $[110]_{\mathrm{MgO}}$ (which corresponds to $[100]_{\mathrm{Fe-Ga}}$) and $[1\bar{1}0]_{\mathrm{MgO}}$ ($[010]_{\mathrm{Fe-Ga}}$) directions, M_r reaches its maximum, while the minima are along $[100]_{\mathrm{MgO}}$ ($[110]_{\mathrm{Fe-Ga}}$) and $[010]_{\mathrm{MgO}}$ ($[1\bar{1}0]_{\mathrm{Fe-Ga}}$). This behavior indicates the presence of a four-fold in-plane magnetic anisotropy. Following the epitaxial relationships found by the RPF study, this M $vs.$ H behavior is related to the cubic symmetry of the magnocrystalline anisotropy when the (100) plane is parallel to the film surface[40]. In Fig. 7(b), we show the hysteresis loops at different in-plane angles for the annealed sample. We have found a similar behavior in this sample compared to the as-grown film, but with somewhat larger values of H_c. The texture study for the annealed sample indicates the presence of a [110] minor phase. This phase should produce a two fold symmetry in the plane of the sample. However the loops for the annealed sample do not reflect such behavior. We will discuss in depth this issue when analysing the FMR results.

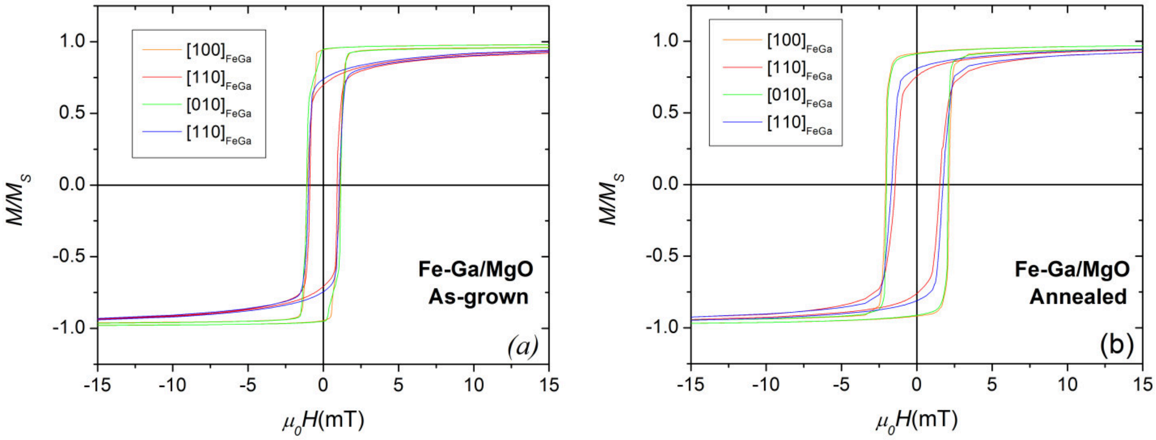

FIG. 7. Hysteresis loops for Fe-Ga/MgO(100) for the (*a*) as-grown and (*b*) annealed samples.

In Fig. 8(*a*), we show the typical FMR spectra for the as-grown and annealed Fe-Ga/MgO samples. Fig. 8(*b*) displays the FMR in-plane H_r angular sweep for the as-grown and annealed Fe-Ga/MgO samples. For both samples we can clearly observe a four fold behavior which is related to the (100) epitaxy determined from RPF. From that figure, it is possible to observe that the variation of H_r as a function of ϕ_H is larger in the annealed sample. This indicates a strong increase in the magnetocrystalline anisotropy after the thermal treatment, probably, due to a better alignment of the grains as a consecuence of the annealing.

In order to quantify the magnetic anisotropy in Fe-Ga/MgO samples, we have modeled the observed dynamic magnetic response by means of FMR using the Smit-Beljers formalism[41] that can be expressed in the following equation:

$$\omega^2 = \frac{\gamma^2}{M_s^2 \sin^2\theta}\left[\frac{\partial^2 U}{\partial^2\theta}\frac{\partial^2 U}{\partial^2\phi} - \left(\frac{\partial^2 U}{\partial\theta\partial\phi}\right)^2\right]\Bigg|_{\theta_{eq},\phi_{eq}}. \tag{1}$$

The gyromagnetic ratio γ is defined as $\gamma = g\mu_B/\hbar$, where μ_B is the Bohr's magneton and the *g*-factor is set to 2.1, as in pure Fe[12]. U is the magnetic free energy related to the system under study. The second derivatives are evaluated at the equilibrium magnetization angles, θ_{eq} and ϕ_{eq}, obtained by minimizing U. For our Fe-Ga/MgO samples we can write U in the following way:

$$\begin{aligned} U(\theta,\phi) = & -\mu_0 \mathbf{H}\cdot\mathbf{M} + \frac{\mu_0}{2}M^2\cos^2\theta \\ & + K_u\cos^2(\phi-\phi_u) - K_n\cos^2\theta \\ & + U_{\mathrm{MCA}}, \end{aligned} \tag{2}$$

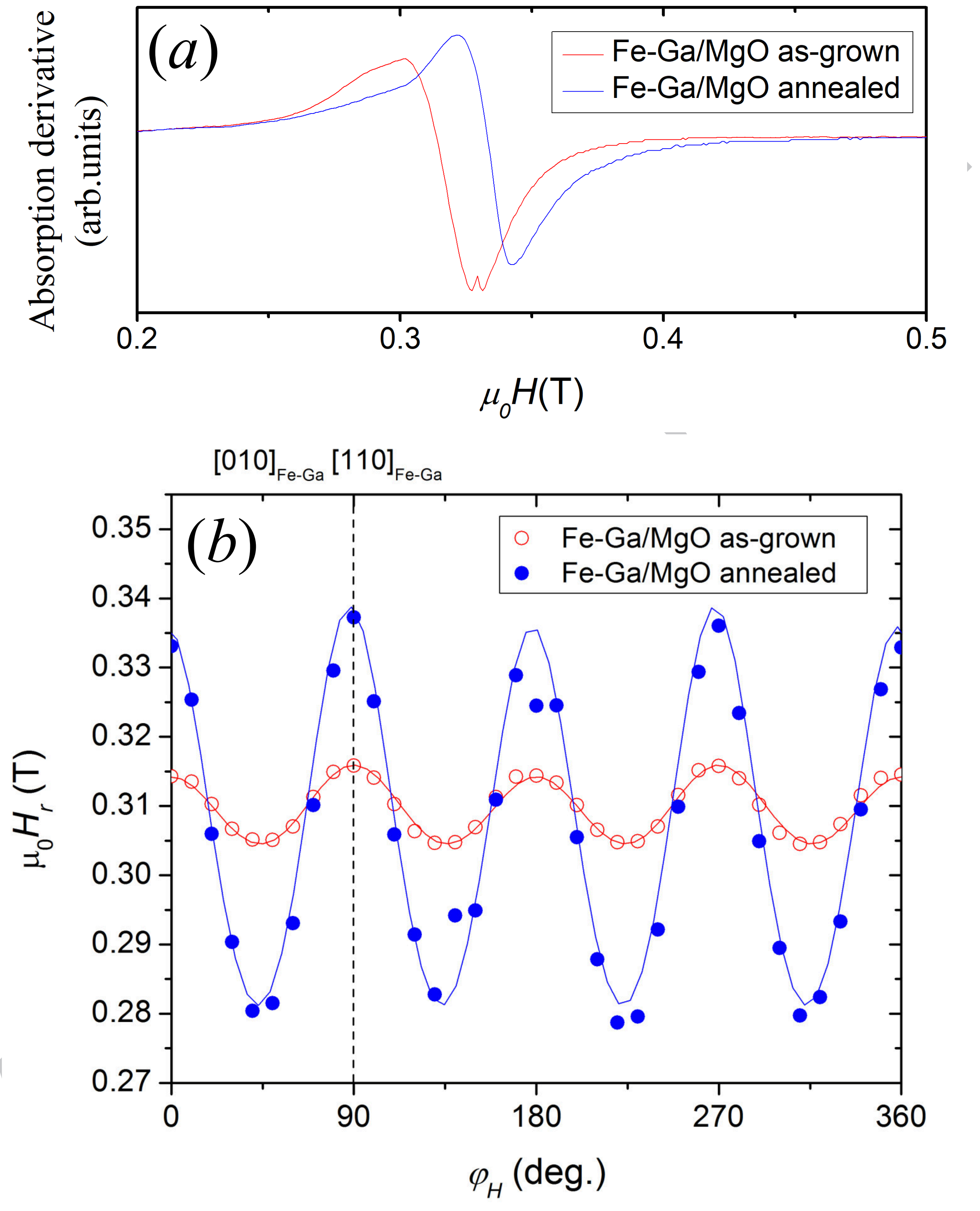

FIG. 8. (*a*) H_r as a function of the in-plane H angle, ϕ_H, for the as-grown (red open circles) and annealed (blue full circles) Fe-Ga/MgO(100) samples. The continuous lines show the calculated resonance fields with the best fitting parameters by using Eqs. (1) and (2). (*b*) FMR spectra for the as-grown (red line) and annealed (blue line) samples $\phi_H = 0°$

where **H** is the applied magnetic field, **M** is the magnetization vector. The first term on the right-hand side is the classical Zeeman energy. The second one is related to the demagnetizing dipolar field, expressed in usual spherical (θ, ϕ) coordinates where the z-axis is perpendicular to the film plane. The third term accounts for a uniaxial in-plane axis related to a small magnetic anisotropy, usually induced during deposition. The four term models the appearence of a uniaxial anisotropy perpendicular to the film, generally related to interfacial effects or residual stress. The last term, U_{MCA}, is related to the cubic magnetocrystalline anisotropy that up to second order can be written as[40]:

$$U_{\mathrm{MCA}} = K_1 \left(\alpha_1^2\alpha_2^2 + \alpha_2^2\alpha_3^2 + \alpha_3^2\alpha_1^2\right), \tag{3}$$

where K_1 is the cubic magnetocrystalline anisotropy constant and α_i are the usual direction cosines of **M** in spherical coordinates, i.e., $\alpha_1 = \cos\phi\, \sin\theta$, $\alpha_2 = \sin\phi\, \sin\theta$, $\alpha_3 = \cos\theta$. The functional form of U_{MCA} depends on the orientation of the crystal with respect to the fixed axes. In our Fe-Ga/MgO samples, according to the texture analysis, we have two different textures as mentioned in Sec. III C. Then, for the as-grown Fe-Ga/MgO sample, which presents only the component texture (100), the corresponding U_{MCA} is:

$$U_{\mathrm{MCA}}^{(100)} = \frac{1}{4}K_1 \left[\sin^2(2\theta) + \sin^4\theta \sin^2(2\phi)\right], \tag{4}$$

which explicitly takes into account that ϕ is the angle between the x axis and a given direction in the film plane and $\phi = 0°$ corresponds to the $[100]_{\mathrm{MgO}}$ ($[1\bar{1}0]_{\mathrm{Fe-Ga}}$) direction. The behavior of the FMR angular sweep in the as-grown sample corroborates the presence of the [100] epitaxy due to the four fold anisotropy observed in the film plane. By fitting the data with Eq. (1), we found that the easy axis of that cubic symmetry is along the $<100>_{\mathrm{Fe-Ga}}$, matching with the behavior observed for bulk Fe-Ga at the same concentration[42]. We have also found that $K_1 = (0.45 \pm 0.01)\times 10^4 \mathrm{J/m^3}$, being one order of magnitude smaller than that expected for bulk Fe-Ga at the same concentration, $K_1^{\mathrm{bulk}} \sim 4.5\times 10^4$ J/m^3 as reported in Ref. 42. This large difference could be ascribed to some misalignment of the magnetic structure that average out the anisotropy for this sample, reducing the resonance field. This fact is also observed in the resonance linewidth for a given direction, where the misalignment produces wider resonance lines due to a larger anisotropy distribution[32]. In our case, the linewidth of the as-grown sample ($\Delta H_r^{\mathrm{a-g}}$ ~50 mT) is larger than that of the annealed one (ΔH_r^{an} ~37 mT). This reinforces the picture of a higher degree of magnetic ordering when the Fe-Ga/MgO is annealed. Moreover, it is possible to observe the presence of two uniaxial anisotropies. On the one hand, the as-grown sample shows a small uniaxial in-plane anisotropy, $K_u = (0.07 \pm 0.01) \times 10^4$ J/m^3, with a hard axis along the $[010]_{\mathrm{MgO}}$ ($\phi_H = 90°$). This anisotropy is generally assigned to a spatial anisotropy during the deposition. On the other hand, the perpendicular anisotropy K_n = (-5±3)$\times 10^4$J/m^3, shows similar values than relaxed films grown onto other insulating substrates[12]. In the case of the annealed sample, it is interesting to note that the weaker texture, (110), was not detected by FMR. We would have e+xpected an additional mode in the resonance spectra that is not present. Probably a strong exchange coupling between both textures makes that only the dominant texture appears in the spectra[39,43]. Then, we use the same magnetocrystalline anisotropy expression than for the as-grown sample. The parameters that best fitted the data are displayed in Table II. Note the increase of the magnetocrystalline anisotropy, $K_1 = (2.25 \pm 0.01) \times 10^4$J/m^3 with respect to the as-grown sample, showing a better magnetic ordering. Finally, the uniaxial parameters, K_u and K_n present values slightly changed with respect to those found in the as-grown sample, presumably, this difference arises either from small changes in the deposition parameters during the growth of both samples or due to the thermal treatment.

TABLE II. Best fitting parameters for the as-grown and annealed Fe-Ga/MgO samples.

Magnetic parameters ($\times 10^4$J/m^3)	Fe-Ga/MgO	
	As-grown	Annealed
K_1	0.45 ± 0.01	2.25 ± 0.01
K_u	0.07 ± 0.01	0.14 ± 0.01
K_n	-5 ± 3	-2 ± 3

IV. CONCLUSIONS

In this work we have studied as-grown and annealed Fe-Ga thin films grown on three different substrates, i.e., glass, Si and MgO with the goal of obtainig different magnetic Fe-Ga behaviors by changing the crystalline Fe-Ga texture. As expected, the structural study shows that the Fe-Ga texture depends on the substrate. Fe-Ga on glass grows without any preferential direction. FeGa/Si(100) presents a small textured volume fraction, with the

{113} family plane directions perpendicular to the film surface. Finally, the MgO crystalline structure determines an epitaxial growth of the Fe-Ga with (100) planes parallel to the substrate surface showing a very good monocrystallinity. When Fe-Ga/MgO(100) is annealed, an additional texture is detected with the (110) plane parallel to the film surface. The magnetic study corroborates the structural results and also puts in evidence that a deep structural analysis is a fundamental tool for a better understanding of the magnetic structure. This work shows that the ability of controling the crystalline texture in ferromagnetic materials gives the possibility of obtaining different magnetic behaviors. This is particularly important in highly magnetostrictive materials, such as Fe-Ga, because it allows to tune their magnetoelastic properties in order to be used in straintronics magnetic devices.

Appendix: ODF calculation using MTEX

The determination of the crystallographic texture is based on describing the orientation (g) of the crystallographic coordinate system of each crystallite with respect to the sample coordinate system. The texture of the sample can then be described by a discrete number of occupation densities in a set of contiguous cells in the orientation space (G-space), containing all possible orientations of the crystallographic system relative to the object system; or equivalently, by a continuous distribution function f(g): the ODF. In practice, the ODF describes how many crystallites presents a given orientation g in the investigated volume of the sample. The orientation distributions are usually represented in 2D density plots in the direct space (pole figures) showing the probability of occurrences of a specific crystal plane normal (hkl) in the Cartesian coordinate system of the sample[44]. Experimentally there are two methods to define the ODF, the ones that measure individual crystallographic orientations directly and the diffraction methods based on the measurements of pole figures using neutron, synchrotron or X-ray diffraction. The diffraction methods requires the determination of the ODF from the experimental pole figures, often referred as the pole figure inversion problem[31]. Over the years, several methods have been proposed an implemented in different computational codes for the resolution of the pole figure inversion problem[31,44–47]. We have employed a novel algorithm for the ODF estimation implemented on the MTEX toolbox, where the estimated ODF is computed as the solution of a minimization problem which is based on a model of the diffraction counts as a Poisson process[48]. The algorithm applies discretization by radially symmetric functions and fast Fourier techniques to guarantee smooth approximation and high performance. In MTEX the ODF is approximated by a superposition of up to 10,000,000 unimodal components. The exact number and position of these components, as well as its shape can be specified by the user. In this work, the positions were chosen equispaced in the orientation space with 5° of resolution and the components are de la Vallee Poussin shaped with the same halfwidth as the resolution of the positions. In quantitative texture analysis, it is often desirable to determine the volume fractions of different texture components, define as: $\frac{dV(g)}{V} = f(g)dg$. The volume fraction of a texture component centred at an orientation g defined by the three Euler angles (ϕ_1, Φ, ϕ_2), is given by[31]:

$$V_f(\phi_1, \Phi, \phi_2) = \int_{\phi_1-\Delta\phi_1}^{\phi_1+\Delta\phi_1} \int_{\Phi-\Delta\Phi}^{\Phi+\Delta\Phi} \int_{\phi_2-\Delta\phi_2}^{\phi_2+\Delta\phi_2} f(\phi_1, \Phi, \phi_2) \sin\Phi \, d\phi_1 \, d\Phi \, d\phi_2. \tag{A.1}$$

In practice, the volume fraction of a texture component located at (ϕ_1, Φ, ϕ_2) is calculated by integrating the value of $f(g)$ within a range of approximately 1.5 times the resolution of the ODF in the orientation space. In the present case, the ODF resolution was 5°, so the volume fraction was calculated using a range of 8°.

ACKNOWLEDGMENTS

The authors gratefully acknowledge R. Benavídes, C. Pérez and M. Guillén for technical support and E. Gayone for fruitful discussions. G. R., J. E. G, A. B., J. M. acknowledges partial financial support by PIP 11220120100250CO, PICT 2013-0401 and SIIP 06/C510.

---

[1] S. Bhatti, R. Sbiaa, A. Hirohata, H. Ohno, S. Fukami, and S. Piramanayagam, Mater. Today **20**, 530 (2017).

[2] E. Du-Tremolet-de Lacheisserie and J. C. Peuzin, J. Magn. Magn. Mater. **136**, 189 (1994).

[3] A. K. Biswas, H. Ahmad, J. Atulasimha, and S. Bandyopadhyay, Nano Lett. **17**, 3478 (2017).

[4] J. Cui, J. L. Hockel, P. K. Nordeen, D. M. Pisani, C.-Y. Liang, G. P. Carman, and C. S. Lynch, Appl. Phys. Lett. **103**, 232905 (2013).

[5] C.-W. Nan, M. I. Bichurin, S. Dong, D. Viehland, and G. Srinivasan, Appl. Phys. Lett. **103**, 232905 (2013).

[6] J. Atulasimha and A. B. Flatau, Smart. Mater. Struct. **20**, 043001 (2011).

[7] C. V. Thompson and R. Carel, J. Mech. Phys. Solids **44**, 657 (1996).

[8] R. Ranchal, S. Fin, and D. Bisero, J. Phys. D Appl. Phys. **48**, 075001 (2015).

[9] M. Eddrief, Y. Zheng, S. Hidki, B. Rache Salles, J. Milano, V. H. Etgens, and M. Marangolo, Phys. Rev. B **84**, 161410 (2011).

[10] A. Javed, N. Morley, and M. Gibbs, J. Magn. Magn. Mater. **321**, 2877 (2009).

[11] M. Barturen, B. Rache Salles, P. Schio, J. Milano, A. Butera, S. Bustingorry, C. Ramos, A. J. A. De Oliveira, M. Eddrief, E. Lacaze, F. Gendron, V. H. Etgens, and M. Marangolo, Appl. Phys. Lett. **101**, 092404 (2012).

[12] M. Barturen, J. Milano, M. Vásquez-Mansilla, C. Helman, M. A. Barral, A. M. Llois, M. Eddrief, and M. Marangolo, Phys. Rev. B **92**, 54418 (2015).

[13] M. Barturen, M. Sacchi, M. Eddrief, J. Milano, S. Bustingorry, H. Popescu, N. Jaouen, F. Sirotti, and M. Marangolo, Eur. Phys. J. B **86**, 191 (2013).

[14] S. Limandri, C. Olivares, L. Rodriguez, G. Bernardi, and S. Suárez, Nucl. Instrum. Meth. B **318**, 47 (2014).

[15] M. Mayer, AIP Conf. Proc. **475**, 541 (1999).

[16] J. Campbell, N. Boyd, N. Grassi, P. Bonnick, and J. Maxwell, Nucl. Instrum. Meth. B **268**, 3356 (2010).

[17] P. Martinez, F. Ruiz, J. Curiale, M. V. Mansilla, R. D. Zysler, L. Dada, M. S. Moreno, L. Rodríguez, D. Fregenal, G. Bernardi, and E. L. Jr, J. Phys. D Appl. Phys. **49**, 335302 (2016).

[18] H. L. Luo, Trans. Metall. Soc. AIME **239**, 119 (1967).

[19] F. Malamud, L. M. Guerrero, P. La Roca, M. Sade, and A. Baruj, Mater. Design **139**, 314 (2018).

[20] F. Malamud, A. M. Riffo, M. V. Alvarez, P. Vizcaino, M. Li, X. Liu, S. Vogel, M. Law, V. Sumin, V. Luzin, R. Vasin, and J. Santisteban, J. Nucl. Mater. **510**, 524 (2018).

[21] R. Hielscher and H. Schaeben, J. Appl. Crystallogr. **41**, 1024 (2008).

[22] R. W. Vook and F. Witt, J. Vac. Sci. Technol. **2**, 243 (1965).

[23] F. Witt and R. W. Vook, J. Appl. Phys. **39**, 2773 (1968).

[24] M. G. Krishna, K. K. Mallick, and A. K. Bhattacharya, J. Mater. Res. **13**, 3221 (1998).

[25] M. Kato, M. Wada, A. Sato, and T. Mori, Acta Metall. **37**, 749 (1989).

[26] C. V. Thompson and R. Carel, Mat. Sci. Eng. B **32**, 211 (1995).

[27] P. B. Barna and G. Radnóczi, “Metallic films for electronic, optical and magnetic applications,” (Woodhead Publishing, Oxford, 2014) Chap. 3.

[28] I. Petrov, P. B. Barna, L. Hultman, and J. E. Greene, J. Vac. Sci. Technol. A **215**, S117 (2003).

[29] Y. C. Feng, D. E. Laughlin, and D. N. Lambeth, J. Appl. Phys. **76**, 7311 (1994).

[30] L. Tang and G. Thomas, J. Appl. Phys. **74**, 5025 (1993).

[31] H. J. Bunge, *Texture Analysis in Materials Science. Mathematical Methods* (Helga and Hans-Peter Bunge, Wolfrathausen, 2015).

[32] A. Butera, J. Gómez, J. L. Weston, and J. A. Barnard, J. Appl. Phys. **98**, 033901 (2005).

[33] M. Ciria, M. G. Proietti, E. C. Corredor, D. Coffey, A. Begué, C. de la Fuente, J. I. Arnaudas, and A. Ibarra, J. Alloy Compd. **767**, 905 (2018).

[34] W. D. Nix, Metall. Trans. A **20A**, 2217 (1989).

[35] N. Kawamiya, K. Adachi, and Y. Nakamura, J. Phys. Soc. Jpn. **33**, 1318 (1972).

[36] A. Muñoz-Noval, A. Ordóñez-Fontes, and R. Ranchal, Phys. Rev. B **93**, 214408 (2016).

[37] J. Varalda, J. Milano, A. J. A. de Oliveira, E. M. Kakuno, I. Mazzaro, D. H. Mosca, L. B. Steren, M. Eddrief, M. Marangolo, D. Demaille, and V. H. Etgens, J. Phys. D Appl. Phys. **18**, 9105 (2006).

[38] J. Gómez, J. L. Weston, and A. Butera, Phys. Rev. B **76**, 184416 (2007).

[39] J. F. Cochran, B. Heinrich, and A. S. Arrott, Phys. Rev. B **34**, 7788 (1986).

[40] B. D. Cullity and C. D. Graham, *Introduction to Magnetic Materials*, 2nd ed. (Wiley-IEEE Press, 2009).

[41] J. Smit and H. Beljers, Philips Res. Rep. **10**, 113 (1955).

[42] S. Rafique, J. R. Cullen, M. Wuttig, and J. Cui, J. Appl. Phys. **95**, 6939 (2004).

[43] P. Schio, M. Barturen, J. Milano, F. J. Bonilla, Y. Zheng, F. Vidal, and A. J. A. de Oliveira, Mater. Res. Express **1**, 035015 (2014).

[44] H. -R. Wenk and P. V. Houtte, Rep. Prog. Phys. **67**, 1367 (2004).

[45] R. -J. Roe, J. Appl. Phys. **36**, 2024 (1965).

[46] S. Matthies, L. Lutteroti, and H. R. Wenk, J. Appl. Crystallogr. **30**, 31 (1997).

[47] S. Matthies, H. -R. Wenk, and G. W. Vinel, J. Appl. Crystallogr. **21**, 285 (1988).

[48] R. Hielscher and H. Schaeben, J. Appl. Crystallogr. **41**, 1024 (2008).